Effects of Zero Net Mass Flux devices on a Next-Generation Tiltrotor airplane in subsonic regime by numerical simulation at high Reynolds number

Abderahmane Marouf, Agathe Chouippe, Dinh Hung Truong, Yannick Hoarau, Dominique Charbonnier, Alain Gehri, Jan B. Vos

Effects of Zero Net Mass Flux devices on a Next-Generation Tiltrotor airplane in subsonic regime by numerical simulation at high Reynolds number

Abderahmane Marouf[1], Agathe Chouippe[1], Hung Dinh Truong[1], Yannick Hoarau[1], Dominique Charbonnier[2], Alain Gehri[2] and Jan B. Vos[2]

[1]*ICUBE laboratory, University of Strasbourg, 02 Rue Boussingault 67000 Strasbourg, France*

[2]*CFS Engineering, EPFL Innovation Park, Batiment A, CH-1015 Lausanne, Switzerland*

Abstract

The flow around the Leonardo Next-Generation Civil Tiltrotor aircraft (NGCTR-TD) is examined in the European research programme CleanSky AFC4TR 'Active Flow Control for Tilt-Rotor aircraft" N° 886718, with the main objective to investigate the use of Active Flow Control Zero Net Mass Flux (ZNMF). This work focuses on the optimization of different parameters such as the frequency of actuation, the velocity, the angle of the jet and the dimensions of the actuators to better reattach the flow through the enhancement of the mixing and momentum transfer within the boundary layer to explore the capabilities of the AFC applicability to a full-scale VTOL aircraft.

1. Introduction

The design of the Next Generation Civil Tilt-Rotor aircrafts (NGCTR-TD) allows an increase of the aerodynamic performance and operational capabilities for civil air transportations. The NGCTR-TD aircraft of Leonardo Helicopters will be able to achieve a cruise speed of more than 500 km/h, double than speed of helicopters and close to regional aircrafts with turboprop engine systems[1]**.** This new, safe and efficient form of aircrafts is required to complete the existing urban transport and to respond to the rapid growing population. This could minimize the environmental footprint of the CO2 and noise emissions and ensures people's mobility. A demonstrator will be constructed with novel architecture, technologies, and systems by Leonardo. In this context, Active Flow Control strategies using Zero Net Mass Flux "ZNMF" devices are being studied to overcome the aerodynamic performance deterioration caused by the flow separation near stall conditions at real flight conditions.

A classification of Active Flow Control devices was summarized in [1]. ZNMF devices belong to the category of fluidic actuators, and the first ZNMF actuator was made to produce waves of acoustics [2] in 1950. Seifert and Pack [3] are one of the pioneers in the studies of the effectiveness of synthetic jets with their experiments of active flow control on a NACA0015 at high Reynolds number at around 10^7. Several following experimental investigations [4,5,6] also confirmed the advantages of using ZNMF to increase the lift and reduce the drag. The influence of synthetic jets was also investigated by many numerical studies using different airfoils summarized in [7,8,9], just to name a few. These studies showed that the jets operate better if they were placed at the separation point to reach the maximum lift, and the effectiveness of the jet was proportional to the jet momentum. Due to the large computational costs and the possible multi-constraints of the objective function, there are only a few studies acquiring optimal parameters of synthetic jets by employing optimization algorithms, to the best of our knowledge. Duvigneau and Visonneau [10] coupled a fluid solver with an optimization procedure in order to reach the optimal performance of a synthetic jet located at 12% chord from the leading edge of a NACA0015 airfoil. Montazer et al. [11] employed the Response Surface Methodology (RSM) method to optimize the jet location, the jet frequency and the jet.

Two-dimensional simulations with constant blowing, sinusoidal blowing and blowing-suction were investigated [12,13], and a novel approach using a coupled AFC with a morphing flap [14] was proposed. The cambering concept as well as trailing-edge vibrations [15] were studied in the European project Smart Morphing & Sensing SMS H2020 leading to optimal performance increase using a specific deformation. However, when the latter becomes important (high deformation) the boundary layer is detached which decreases the aerodynamic efficiency. The AFC could re-attach the boundary layer, enhance the pressure distribution, and therefore increase the wing performance.

The paper presented here focuses on the use of Active Flow Control for two and three-dimensional configurations allowing to optimize different parameters of the jet such as the influence of the velocity, frequency, dimension, orientation, and location of the ZNMF actuators regarding the separation of the boundary layer. Both approaches will help to analyze furthermore the AFC towards the real scale NGCTR aircraft at near stall conditions. Section 2 describes

the numerical methods such as the code used in the study which allows to simulate the AFC, then different configurations and their descriptions regarding the domain, the mesh generation and turbulence modelling. Section 3 examines the influence of the jet speed, the frequency, the location, and the dimensions of the jet such as the diameter and the angle. Based on these results the Delayed Detached Eddy Simulation (DDES) approach is used for 3D simulations to reveal the near wake coherent structures and the interaction between the separated boundary layer and both the wing and the flap's shear-layers in addition to the added jet. Finally, optimal parameters are selected to examine the AFC effects towards a full NGCTR aircraft for two different flight configurations at near stall conditions.

2. Numerical methods

2.1 NSMB solver

The Navier Stokes Multi Block solver NSMB [16,17] is used in this study. The code employs the cell-centred finite volume method with multi-block structured grids to solve the compressible Navier Stokes equations. In the context of this project, the Chimera and patch grid generation methods are used and available to consider the movement of different parts. Low and high order space discretization schemes exist in the code such as the 2^{nd} and 4^{th} order central scheme, Roe and AUSM upwind schemes from 1^{st} to 5^{th} order. Explicit Runge-Kutta schemes and semi-implicit LU-SGS are used for time discretization. In this study, we used the 1^{st} order central scheme for space and implicit dual time stepping discretization. The NSMB code offers a large choice of turbulence modelling such as (U)RANS and hybrid RANS-LES, as for example Delayed Detached Eddy Simulation (DDES) [18]. The Spalart Allmaras (SA) [19] has been used for the 2D unsteady simulations and for the NGCTR aircraft, while for 3D high-lift wing-flap system with a fixed span, the DDES-SA is employed.

The ZNMF actuators are simulated using a small cavity with an imposed sinusoidal velocity with a blowing-suction methodology. The parameters of the jet condition permit the variation of the dimension such as its location, diameter, and orientation, in addition to the jet velocity and frequency.

2.2 High-lift wing-flap system

A high-lift system with a wing-flap two elements prototype is considered. The grid of the prototype in the wind tunnel is generated (figure 1). The chimera method is used to allow a quick flap deflection. Three levels of grids are defined as follows: the first presents the full domain including the wind tunnel walls and the wing. A second grid is created as an O-mesh type and contains only the main wing. Finally, the flap is considered as a separated part to facilitate the deflection procedure for different flight stages as for example in take-off and landing configurations.

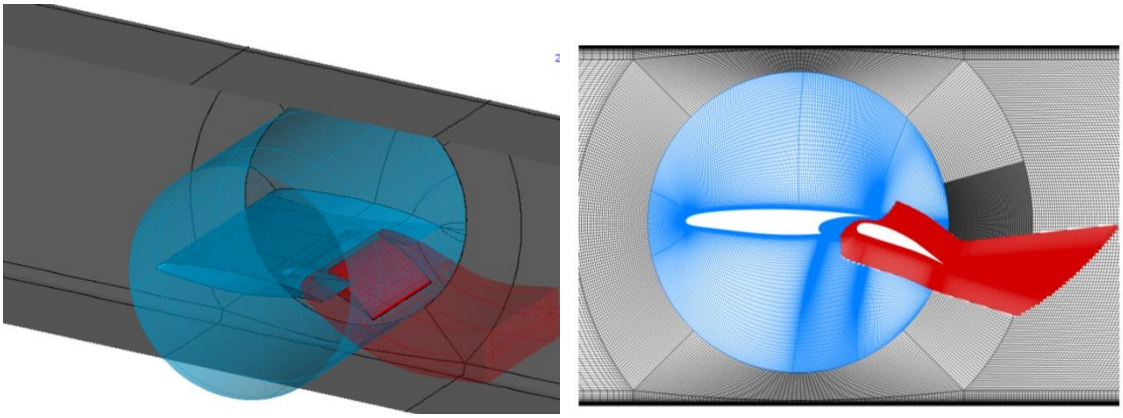

Figure 1: (left) the CAD design of the high-lift system inside the wind tunnel, (right) the structured grid of the large-scale prototype in landing conditions with an AoA of 2° and flap deflection of 25°

To control the flow separation located on the morphing flap using the cambering approach at higher amplitudes of deformation and at high angles of deflection with an objective to increase the aerodynamic efficiency, several strategies exist for the modelling of ZNMF devices. Some techniques model the jet as boundary condition, others include the movement of the membrane (movement of pistons). Gallas [20] performed experimental and numerical studies of a

ZNMF actuator and demonstrated that to capture the correct flow physics of the jet flow, it was necessary to model the plenum cavity of the actuator. A set of simple Modified Boundary Conditions (MBC) were proposed by [21] to model the ZNMF device. This study showed promising results but was limited to 2D incompressible flows. A literature survey showed that modelling of the cavity plenum is important, in particular in 3D, and it was decided to model ZNMF actuators including the plenum using the chimera grid modelling approach (figure 1).

The chimera grid fits the surface of the wing and replaces the original grid in the simulation. The refinement of this chimera grid on the wing will be similar as to the one of the domain to reduce interpolation errors as well as the numerical dissipation between both levels of grids. This methodology enables to correctly capture the flow physics (figure 2) and it provides a very simple environment to modify the orientation, location, and the dimensions of the jet flow device on the configuration. The flow movement in the plenum cavity can be obtained by oscillating the cavity bottom wall or with an imposed velocity boundary condition. However, the oscillation of the cavity will induce deformation of cells that may modify the velocity profiles inside the boundary layer. An imposed periodic velocity is proposed as alternative solution to simulate a similar behaviour of the ZNMF device. In this study, as a first step, the cavity is not considered and only the exit jet has been inserted into the flap's grid, to optimize several parameters (velocity and frequency) for the delay and suppression of the separation

2.3 Next Generation Tiltrotor NGCTR-TD aircraft

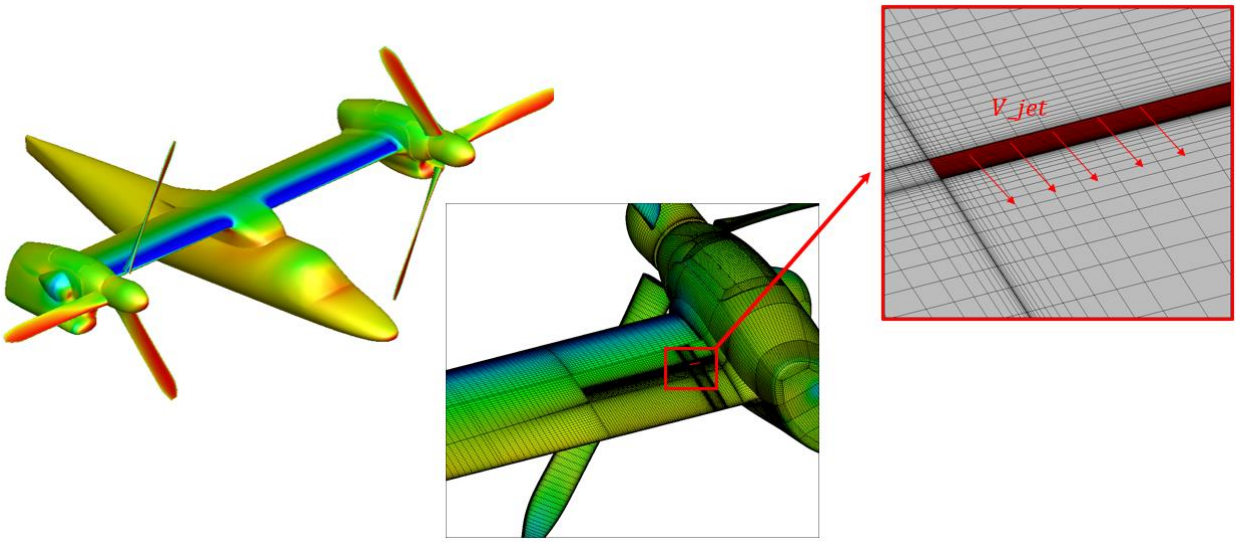

Figure 2: Example of an embedded jet near the nacelle-wing junction

Different grids with jets were prepared by CFS-Engineering using the Chimera (over set) method for these 2 configurations in 2 different flight conditions with and without aileron deflection. The jets are added to the existing mesh (figure 2). They can be oriented/translated in all the wing-aileron surfaces without any remeshing because they are in separated blocks using a patched grid. Figure 2 (middle and right) highlights an example of the integration of one jet near the wing-nacelle junction.

3. Results

3.1 Two-dimensional simulations using high-lift wing-flap system

The jet actuation frequency has an important role because real ZNMF actuator devices have optimal bandwidth frequencies. The blowing-suction jet interacts with the boundary layer and the flow separation. Numerical simulations were made for different jet velocities and actuation frequencies, and the results are summarized in figure 3. When the jet velocity is increased (indirect increase of the jet momentum), the flow separation is better delayed, and an efficient control can be obtained. This results in a decrease of drag up to -29% and an increase in lift by +2.85%, leading to a substantial increase in aerodynamic efficiency.

The aerodynamic coefficients presented in figure 3 also show that the flow becomes less sensitive to the actuation frequency for frequencies above 100 Hz. The lift and drag coefficient are approximately constants when the frequency of actuation is higher than 100 Hz.

Cases	C_l	C_d	Lift-to-Drag
70m/s			
20Hz	-5.2%	-5.7%	-7.6 %
50Hz	-4.9%	-5.6%	-7.4 %
100Hz	-5.7%	-6.03%	-7,74 %
150Hz	-6.19%	-5.7%	-8.5%
200Hz	6.187%	-5.45%	-8.9%
100m/s			
20Hz	-4.75%	-13.7%	1.4%
50 Hz	-4.61%	-13.65%	1.41%
100Hz	-4.79%	-14.32%	2.16%
150Hz	-3.4%	-13%	2.15%
200Hz	-3.8%	-12.83%	1.46%
150m/s			
20Hz	-1%	-21.53%	15.9%
50Hz	-0.93%	-22.2%	17.1%
100Hz	-2.27%	-24.7%	19.39%
150Hz	-1.01%	-23.35%	18.73%
200Hz	-2.67%	-24.48%	18.49 %
200m/s			
20Hz	2.55%	-24.15%	24.95%
50Hz	3.2%	-25.26%	26.95%
100Hz	2.63%	-26.9%	29.2%
150Hz	2.23%	-27.45%	29.54%
200Hz	2.85%	-26.7%	29.05%

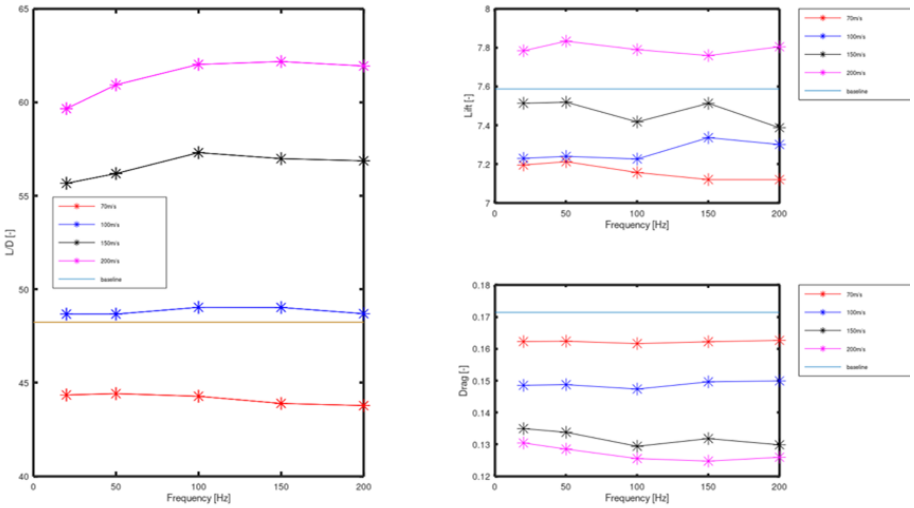

Figure 3: Gain/loss the aerodynamic efficiency and in lift and drag coefficients as a function of the jet frequency

The jet location is one of the most important parameters which should be well examined and optimized. An important reattachment of the flow can be obtained when the jet locations are well adapted. However, to our knowledge, the optimal jet location depends on the location of the flow separation and there is no general optimal jet location applicable to all the configurations such as 2D/3D wings, high-lift systems, swept wings and full aircraft with junctions. The location of the flow separation depends on the flow conditions (initial and boundaries) and the geometry.

Figure 4 shows the effect of the jet location for the case with a known location of the separation point. The jet location was selected at four stations upstream and near the separation point. The results show that when the jet is close to the separation point, it has a large efficiency. However, when the jet location is upstream (before separation) and a certain distance from the separation the effects are less important. This can be explained by the dissipation of the jet and loss of energy when the jet travels towards the separation point.

Location (%c)	C_l	C_d	Lift-to-Drag
50	-1.96%	-15.63%	6.83 %
55	-1.33 %	-18.31%	11.04 %
65	-0,46%	-19.22%	13.2 %
70	-0.02%	-23.17%	19.56%

Figure 4: Different locations of the jet with respect to the separation location and their effects on the aerodynamic coefficients and the aerodynamic efficiency, jet velocity 200 m/s, jet dimensions 45°, 1mm

Different dimensions and orientations of the jet were selected based on a real existing piezo actuator developed by ONERA (presented in the previous section). The piezo-actuator dimensions have a 1mm jet exit, with a 45° orientation with respect to the free-stream flow. For a fixed mass flux, the jet exit dimension and orientation were varied, leading to different jet velocities. Figure 5 summarizes the different configurations studied and highlights the influence of jet exit dimension and orientation on the lift and drag coefficients.

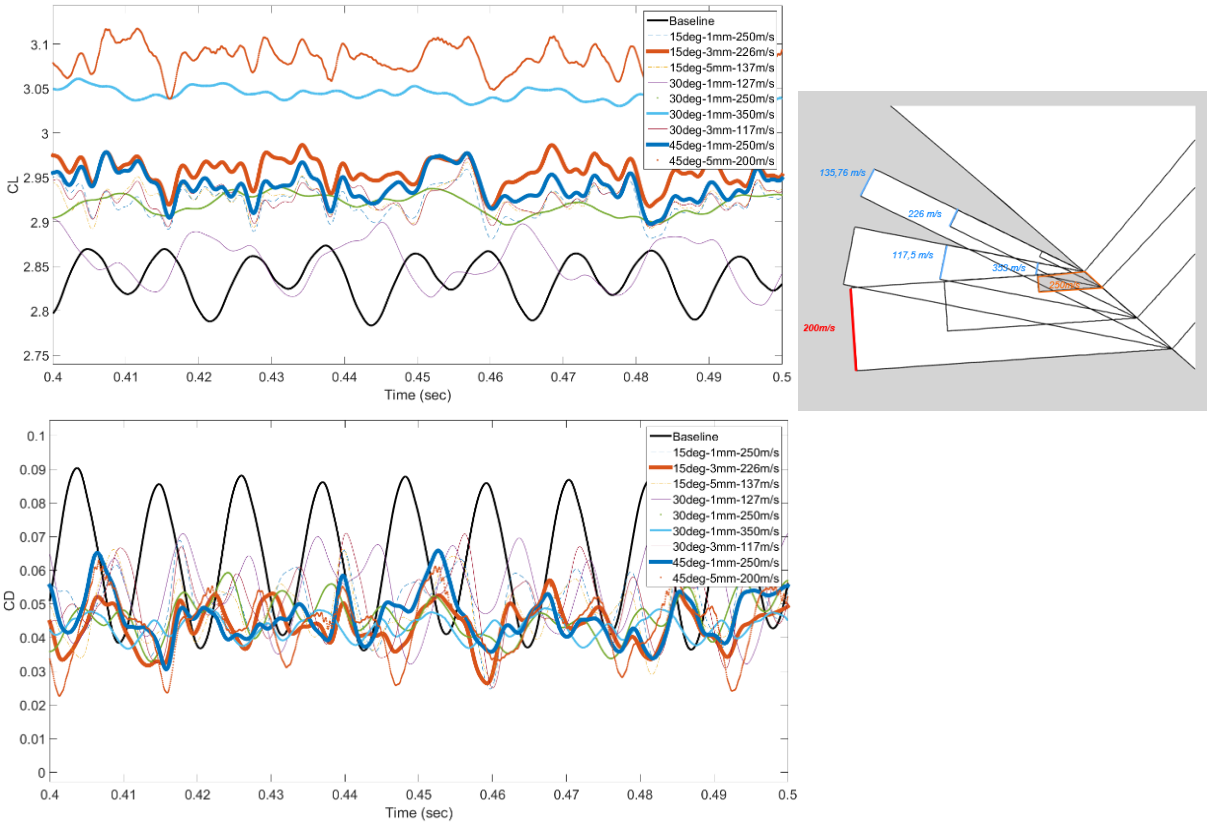

Figure 5: Representation of different dimensions and orientations of the jet, and their effects on the aerodynamic lift and drag coefficients using a fixed mass flux based on a realistic ZNMF piezo-actuators ASPIC

Continuous blowing with $\frac{V_{jet}}{U_\infty} \geq 1.5$ completely suppresses the adverse pressure gradient and restores a positive velocity profile in the inner boundary layer. Pulsed blowing showed the additional effects of low and high frequencies of periodic jets and optimal frequencies. Blowing-Suction approach using ZNMF jets has been examined and different parameters are investigated: The influence of the jet on the aerodynamic forces becomes independent of the jet actuation frequency for actuation frequencies > 100Hz. For the different jet velocities studied it was shown that the highest jet velocity gave the largest increase in aerodynamic efficiency.

The position of the jet should be located upstream of the separation point to permit the flow to reattach.

Based on existing ZNMF actuators (ONERA), a shape optimisation of the angle with D/H of the ZNMF actuator was investigated for a fixed mass flow. In terms of increased aerodynamic efficiency, the best results were obtained for a jet angle of 15°.

3.2 Three-dimensional simulations using high-lift wing-flap system (DDES approach)

The SA model was able to predict the flow separation from the higher cambering coupled with high angles of deflection of the flap. The use of hybrid RANS/LES model (DES) is set by the grid cells, so in thicker boundary layer zones, as for instance a presence of a flow separation, the standard DES may be affected by the Modelled Reynolds Stress Depletion issue [19]. To delay the switch to the LES and to treat the entire boundary layer with a URANS model, we use the DDES which provided good results studies for the same configuration at take-off position previously investigated in [22, 23, 24]. A multi-block structured mesh of ≈40 million cells was carefully prepared and adapted to the hybrid model. The implicit dual time stepping approach with a time step of $\Delta t=10-5$ seconds was used to accurately resolve the small-scale structures on this adapted grid

The second test case considers a smaller spanwise length (0.27m) using an adapted grid with the hybrid turbulence model DDES-SA. The detached turbulent flow contains smaller chaotic structures that are resolved using the LES model, in addition to the coherent structures considered as large eddies displaying a regular flow pattern in the near area of the trailing edge region. The comparison in figure 6 shows that the Q-criterion clearly exhibits the flow detachment locations. Anti-clockwise vortices are formed past the flap's trailing edge, due to the high cambering and deflection angle. These vortices extend along the vertical direction through their interactions with the separated upper shear-layer of the flap. These large eddies are presumed as the coherent shedding vortices. The upper and lower shear-layer coming from the wing interact directly with the separation, this will lead to a strengthening of the interaction between the flap's and the wing's shear-layers leading to a considerable growth of the width of the wake. The separation (figure 6(a) in blue)

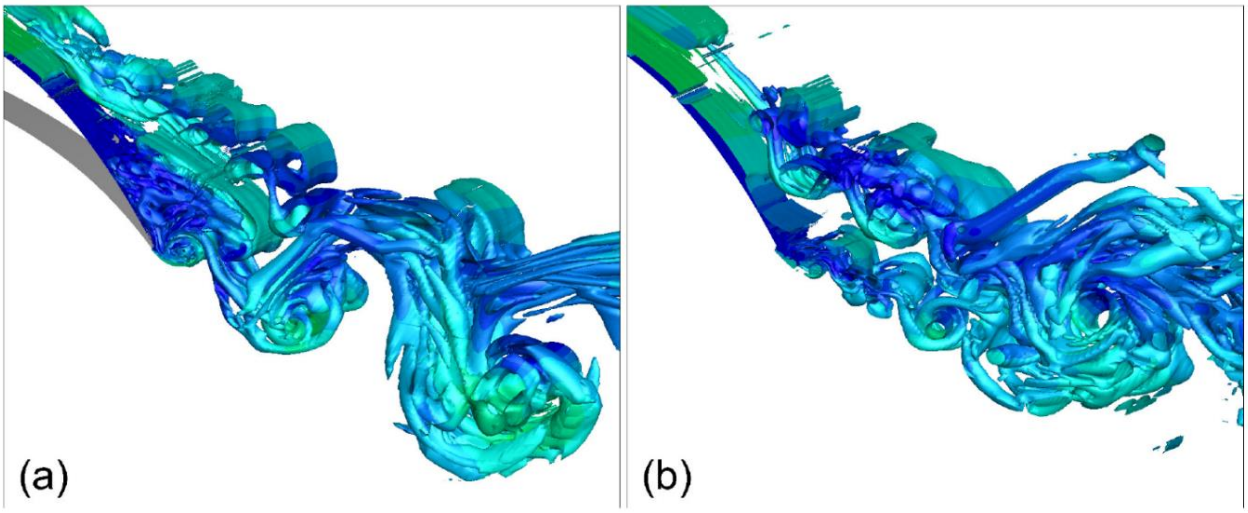

Figure 6: Snapshot of the Q-criterion showing the region of flow separation in blue (a) located at approximately 58% of the flap's chord and the attenuation of the separation (b) by using the Active Flow Control with ZNMF with the periodic induced blowing-suction jet at a speed of $Vjet/U\infty$ = 2.9 and a frequency of F+=2.38.

located at approximately 58 % of the flap's chord has been attenuated (figure 6(b)) in the case of the Active Flow Control with ZNMF by the periodic induced blowing-suction jet at a speed of $Vjet/U\infty$=2.9 and a frequency of $F+$=2.38. The injected jet increases the boundary layer momentum thickness. As a result, the separation moves downstream towards the trailing edge. The pressure distribution is enhanced along the separated area of the flap due to the reattachment of the flow. Both shear-layers of the wing and the flap are highly affected by the ZNMF jet. This last induces a complete disappearance of the anticlockwise vortices formed past the trailing-edge of the flap, because of the reattachment of the flow. The interaction between both shear-layers is then delayed and weakened. The pressure enhancement and the wake thinning will lead to an important modification of the flow behaviour around the high-lift system and will result in improving the aerodynamic efficiency.

3.3 Active Flow Control for the Next Generation Tilt-Rotor aircraft

At the start of the studies several of simulations were carried out using a steady blowing strategy for different jet velocities with only one integrated jet near the aileron-nacelle junction. Figure 7 highlights the near aileron-nacelle region with the jet and the existing corner vortex both interacting together. The size of this vortex decreases with the increase of the jet velocity due to the enhancement of the boundary layer momentum, which enforces the flow to reattach. The corner vortex is then pushed downstream towards the trailing-edge area. The blue region represents the separation because of the negative values of the friction coefficient CFx component. At high jet velocities, this region is attenuated, and the flow is re-attached

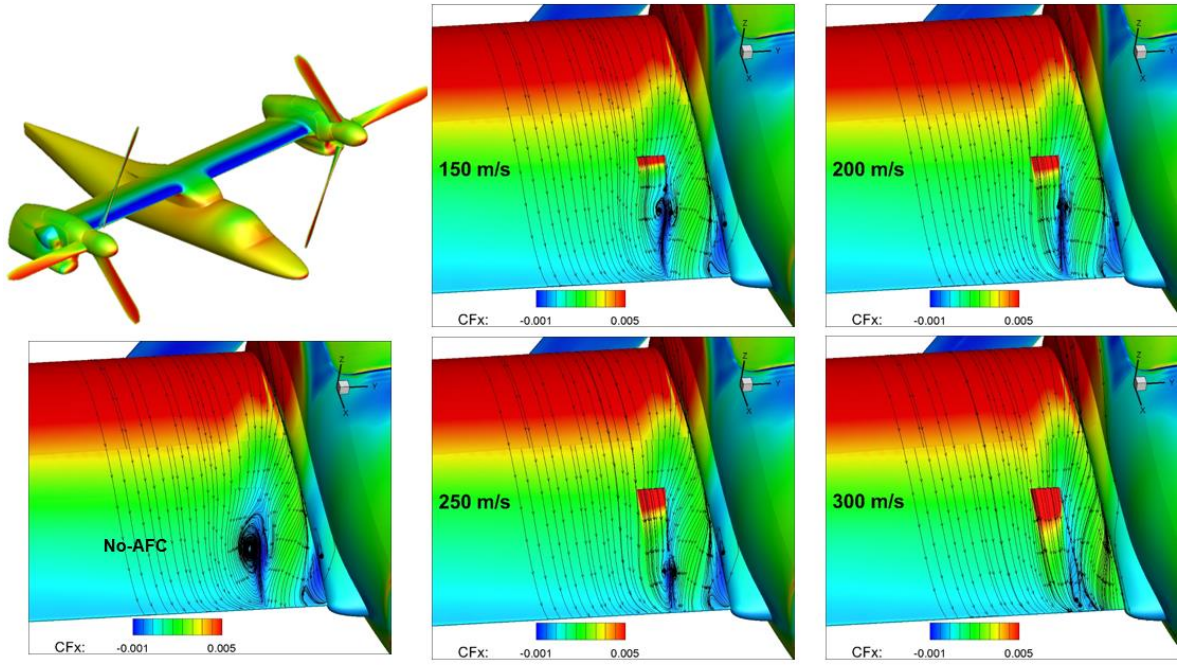

Figure 7: Steady jet control using different jet velocities in the location of the wing-nacelle junction.

Before making detailed studies of Active Flow Control using ZNMF devices, the time step and the tolerance were investigated. Figures 8 and 9 presents the lift and drag coefficients respectively for different time steps and different minimum fixed tolerances using a ZNMF with a jet velocity of 300 m/s and a frequency of 65Hz. Note that all simulations were made with a rotating propellor (3 blades). When the time step is set at dt = 1e-4 associated with a tolerance of 1e-2, important non-physical peaks are captured in both drag and lift signals. When the tolerance is decreased to 1e-3 and time step is fixed to 1e-4 and 5e-5 sec, the over estimation of theses peaks disappeared. Both cases with same tolerance and different time steps provide similar evolutions of the coefficients. Therefore, we judged the case with a time step of 1e-4 sec and a tolerance 1e-3 is well converged and could be appropriate to handle simulations with ZNMF while maintaining good accuracy and reasonable time of simulations.

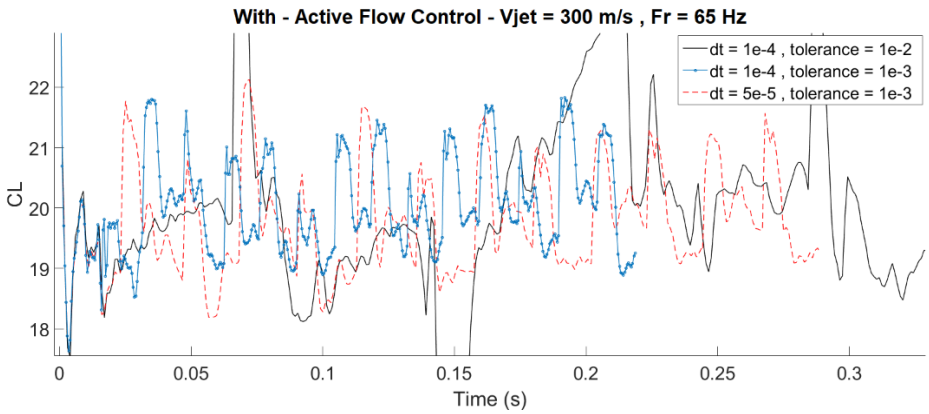

Figure 8: drag and lift coefficient evolution over time for different time steps and tolerances.

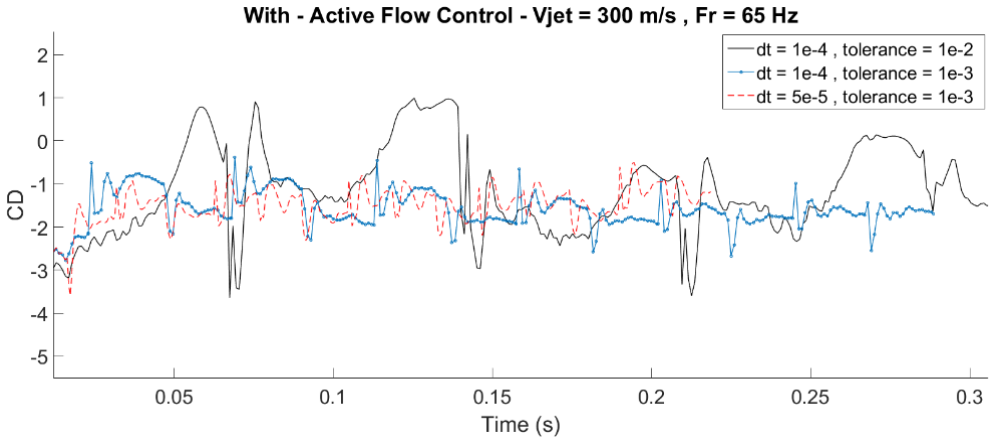

Figure 9: drag and lift coefficient evolution over time for different time steps and tolerances.

Figure 10 highlights the Power Spectral Density (PSD) of the drag coefficient for the same test cases that were presented above.

To predict the predominant frequency of one rotating blade that can be calculated by f_b (Hz)= 2π (rad/s) = 60 rpm. In this case the rotation of blades is fixed. The corresponding blade frequency f_b (Hz)=7.966. The NGCTR contains 3 blades, the total frequency is equal to f_b = 23,9 Hz. The first case with dt=1e-4 sec and tolerance = 1e-2 was not able to capture the corresponding frequency, but for both cases with dt=1e-4 & tolerance 1e-3 and dt=5e-5 & tolerance = 1e-3 captured approximately the same frequency. The frequency of the jet is also captured in the PSD by both cases. Unsteady simulations with ZNMF are conducted with the corresponding time step dt=1e-4 and tolerance 1e-3 that are judged satisfactory.

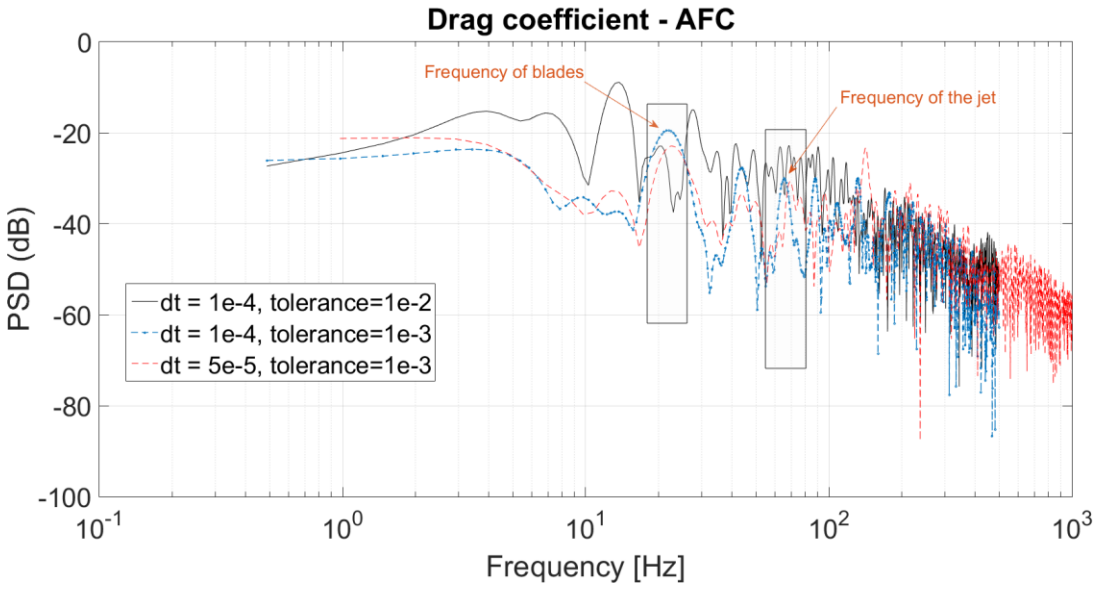

Figure 10: Power Spectral Density of the drag coefficient for different time steps and tolerances.

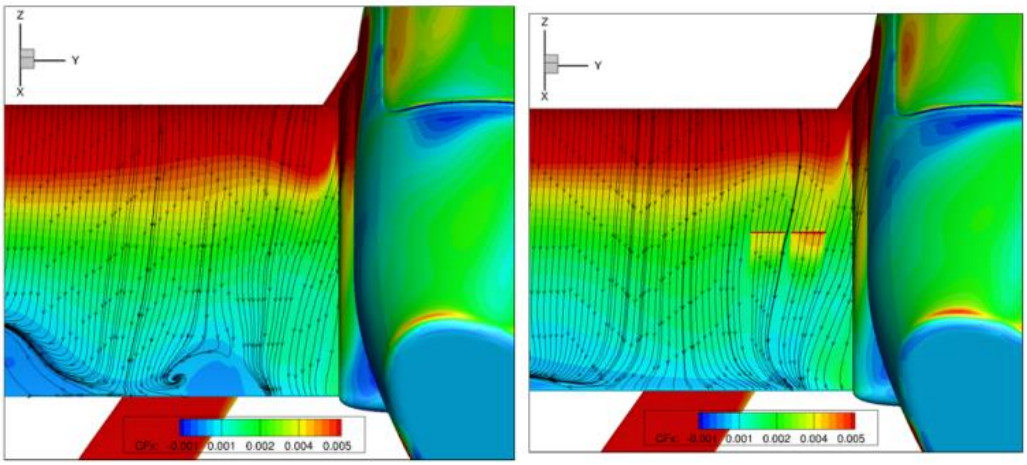

Figure 11: Skin friction coefficient (Cf x) on the aileron for the NGCTR aircraft, (left) baseline (no-control), (right) using 2 ZNMF in the near wing-nacelle junction.

Unsteady simulations were carried out for different configurations. The first case has a closed gap near the aileron, the nacelle was oriented horizontally, and contains ZNMF devices embedded in different regions near the fuselage-wing junction, the middle of the span and the aileron-nacelle junction. Figures 11 (left) presents the reference case without any control, showing the corner vortices and the trailing-edge separation interacting all together. Figure 11(right) shows the results for the calculations with ZNMF devices having a jet velocity of 350 m/s and a frequency of 65 Hz. The dimensions of a single jet are 1mmx150mm, and the mass flux corresponds to the one of the existing piezo-ZNMF actuators (ASPIC) developed by the ONERA. It can be noticed that the flow is reattached in the location of the aileron-nacelle junction leading to a disappear of the corner vortex and to reduce the trailing-edge separation formed along the spanwise direction. The junction aileron-nacelle is highly affected by the location of the two ZNMF jets. The induced periodic jets interact with the corner vortex and push this last downstream towards the trailing-edge. As a result, the separation disappears when the aileron is set at 0° degrees of deflection. The effectiveness of the aileron is improved regarding these ZNMF locations.

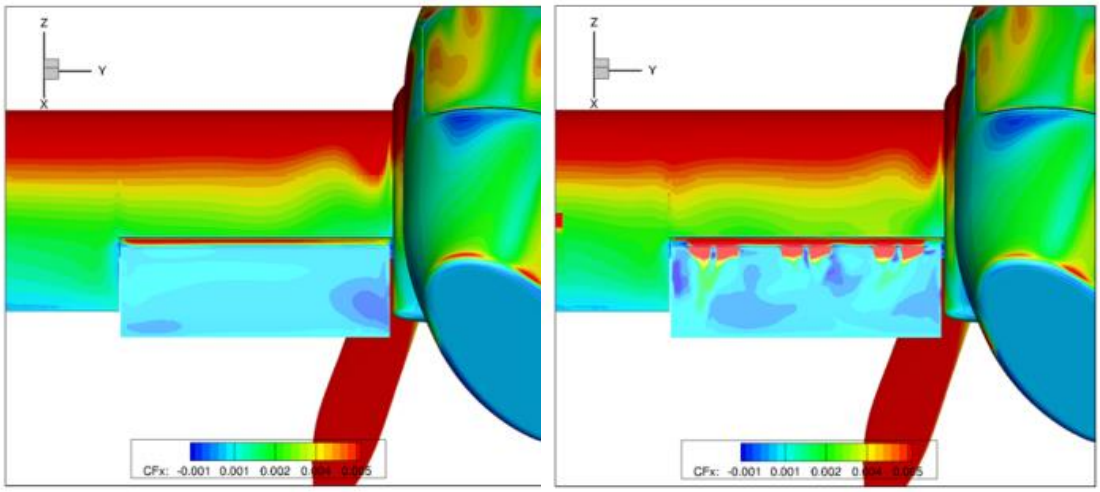

Figure 12: Skin friction coefficient (Cf x) on the aileron for the NGCTR aircraft, (left) baseline (no-control), (right) using 6 ZNMF devices along the aileron span.

The 2nd case has a small gap between wing and aileron, the aileron is deflected downwards, and the nacelle is also in horizontal position. Simulations were made at high angle of attack. At these conditions the flow remains attached along the span of the wing and is less sensitive to the rotation of the blades, however the flow around the aileron is fully detached according to the figure 12 (left). We placed 6 ZNMF jets in the leading-edge area of the aileron presented in figure 12 (right). Figure 12 shows the x-component of the instantaneous skin friction vector for different positions of the ZNMF devices, and one can clearly observe the locations of the ZNMF devices. A delay in flow separation can be

observed through the increase of the friction coefficient. This leads to an important increase of the aerodynamic efficiency up to 12-13% in lift-to-drag ratio of the aileron forces. The maneuverability of the aircraft will be better enhanced through the increase of the aileron efficiency.

4. Conclusions

Simulations using Zero Net Mass Flux devices for Active Flow Control were presented for several configurations. The 2D studies provided: the optimal actuation frequency, the recommended jet velocity, D/H, jet angle and the recommended location of the ZNMF to improve the aerodynamic performance. The 3D DDES-SA simulations revealed the interaction between the separation and the both shear-layers and the AFC effects on these coherent instabilities. Finally the NGCTR-TD aircraft has been investigated using the same code. Different critical configurations were selected to increase their efficiency and delay the detachment of the boundary layer mainly on the wing and the aileron surfaces. Steady blowing with different jet velocities was employed near the aileron-nacelle junction and an optimal jet velocity has been obtained by considering the limitation of the mass flux in the existing actuators. Different numerical parameters were examined such as the optimal time step and the tolerance of the unsteady simulations under the ZNMF active flow control. Unsteady simulations w/o control are investigated using a defined location of the ZNMF jets. The jets interact with the separation and partial reattachment of the flow can be obtained. Corner vortices and trailing-edge separation are attenuated and the aileron efficiency can be enhanced up to 12-13% regarding the lift-to-drag ratio.

5. Acknowledgments

The results presented in this paper are carried in the CleanSky2 project AFC4TR (funded by the European Union H2020 program under Grant Agreement 886718) and the H2020 project SMS (under Grant Agreement 723402). This work was granted access to the HPC resources of [CINES/TGCC] under the allocations 2020-2021-2022-[A0102A11355] and [A0102A05140] made by GENCI. The authors would like to acknowledge the High-Performance Computing Center of the University of Strasbourg for supporting this work by providing scientific support and access to computing resources. Part of the computing resources were funded by the Equipex Equip@Meso project (Programme Investissements d'Avenir) and the CPER Alsacalcul/Big Data. Leonardo Helicopters is acknowledged for providing the geometry of the Next Generation Tilt-Rotor Technology Demonstrator, calculation conditions and their support in performing the simulations.

References

[1] Cattafesta, L.N., Sheplak. M. 2011 - Actuators for Active Flow Control. *Annu. Rev. Fluid Mech*., vol. 43, pp. 247-272.

[2] Ingard, U., and Labate, S. 1950. Acoustic circulation effects and the nonlinear impedance of orifices, *The Journal of the Acoustical Society of America*, Vol 22.

[3] Seifert, A., and Pack, L. G. 1999. Oscillatory Control of Separation at High Reynolds Numbers AIAA Journal, Vol. 37, No. 9, pp. 1062–1071. https://doi.org/10.2514/2.834

[4] McCormick, D. 2000. Boundary layer separation control with directed synthetic jets. In: 38th Aerospace Sciences Meeting and Exhibit, AIAA. https://doi.org/10.2514/6.2000-519

[5] Tuck, A., and Soria, J. 2004. Active flow control over a NACA 0015 airfoil using a ZNMF jet. In: 15th Australasian Fluid Mechanics Conference. The University of Sydney, pp. 00178

[6] Tang, H., Salunkhe, P., Zheng, Y., Du, J., and Wu, Y. 2015. On the use of synthetic jet actuator arrays for active flow separation control. Experimental Thermal and Fluid Science. Vol. 57, pp. 1–10. https://doi.org/https://doi.org/10.1016/j.expthermflusci.2014.03.015

[7] Donovan, J., Kral, L., and Cary, A. 1998. Active flow control applied to an airfoil. In: 36th AIAA Aerospace Sciences Meeting and Exhibit, AIAA. https://doi.org/10.2514/6.1998-210

[8] You, D., and Moin, P. 2008. Active control of flow separation over an airfoil using synthetic jets. J. Fluids. Struct. Vol. 24, No. 8, pp. 1349–1357. https://doi.org/https://doi.org/10.1016/j.jfluidstructs.2008.06.017.

[9] Kim, S. H., and Kim, C. 2009. Separation control on NACA23012 using synthetic jet. Aerosp. Sci. Technol. Vol. 13, No. 4, pp. 172–182. https://doi.org/https://doi.org/10.1016/j.ast.2008.11.001

[10] Duvigneau, R., and Visonneau, M. 2006. Optimization of a synthetic jet actuator for aerodynamic stall control. Comput. Fluids. Vol. 35, No. 6, pp. 624–638. https://doi.org/https://doi.org/10.1016/j.compfluid.2005.01.00

[11] Montazer, E., Mirzaei, M., Salami, E., Ward, T., Romli, F., and Kazi, S. 2016. Optimization of a synthetic jet actuator for flow control around an airfoil. In: IOP Conference Series: Materials Science and Engineering. Vol. 152, p. 012023. https://doi.org/10.1088/1757-899X/152/1/012023.

[12] Marouf, A., Chouippe, A., Vos, J. B., Charbonnier, D., Gehri, A., Braza, M., and Hoarau, Y. Unsteady CFD simulations for Active Flow Control. 2021. *American Institute of Aeronautics and Astronautics*, AIAA. https://doi.org/10.2514/6.2021-2854

[13] Marouf, A., Truong, H.D., Hoarau, Y., Gehri, A., Charbonnier, D., Vos, J.B., and Braza, M. CFD simulations of active flow control devices applied on a cambered flap. AIAA 2022-1545, Session: Applied Computational Fluid Dynamics III Published Online:29 Dec 2021https://doi.org/10.2514/6.2022-1545

[14] Bmegaptche, Y. T., Giraud, A., Jodin, G., Nadal, C., Marouf, A., Martinez, I. G., Harribey, D., Nogarede, B., Rouchon, J.-F., and Braza, M., "Design of a Large-Scale High-Lift Morphing A320 Wing Based on Electro-Mechanical Actuators and Shape Memory Alloys. 2019. American Institute of Aeronautics and Astronautics. https://doi.org/10.2514/6.2019-2908

[15] Marouf, A., Tekap, Y. B., Simiriotis, N., Tô, J.-B., Rouchon, J.-F., Hoarau, Y., and Braza, M., "Numerical investigation of frequency-amplitude effects of dynamic morphing for a high-lift configuration at high Reynolds number," International Journal of Numerical Methods for Heat & Fluid Flow, Vol. 31, No. 2, 2020, pp. 599–617. https://doi.org/10.1108/hff-07-2019-0559

[16] Vos, J., Rizzi, A., Corjon, A., Chaput, E., and Soinne, E. 1998. Recent advances in aerodynamics inside the NSMB (Navier Stokes Multi Block) consortium. *36th AIAA Aerospace Sciences Meeting and Exhibit*, 1998. https://doi.org/10.2514/6.1998-2

[17] Hoarau, Y., Pena, D., Vos, J. B., Charbonnier, D., Gehri, A., Braza, M., Deloze, T., and Laurendeau, E. Recent Developments of the Navier Stokes Multi Block (NSMB) CFD solver. *54th AIAA Aerospace Sciences Meeting*, 2016. https://doi.org/10.2514/6.2016-2056

[18] Spalart, P. R., Deck, S., Shur, M. L., Squires, K. D., Strelets, M. K., and Travin, A. 2006. A New Version of Detached-eddy Simulation, Resistant to Ambiguous Grid Densities. Vol. 20, No. 3, pp. 181–195. https://doi.org/10.1007/s00162-006-0015-0

[19] Spalart, P., and Allmaras, S. A one-equation turbulence model for aerodynamic flows. 1992. 30th Aerospace Sciences Meeting and Exhibit, American Institute of Aeronautics and Astronautics,. https://doi.org/10.2514/6.1992-439

[20] Gallas, Q., "On the modeling and design of zero-net mass flux actuators," Ph.D. thesis, University of Florida, Dec. 2004.

[21] Aram, E., Mittal, R., and Cattafesta, L., "Simple Representations of Zero-Net Mass-Flux Jets in Grazing Flow for Flow-Control Simulations," International Journal of Flow Control, Vol. 2, 2010, pp. 109–125

[22] Marouf, A., "Analyse physique de concepts du morphing électroactif pour accroître les performances aérodynamiques des ailes du futur par simulation numérique de Haute Fidélité et modélisation de la Turbulence à nombre de Reynolds élevé," Ph.D. thesis, 2020. URL https://www.theses.fr/s184078, thèse de doctorat dirigée par Hoarau, Yannick et Braza, Marianna, Mécanique Des Fluides, Université de Strasbourg 2020.

[23] Marouf, A., Hoarau, Y., Vos, J. B., Charbonnier, D., Tekap, Y. T. B., and Braza, M. 2019. Evaluation of the aerodynamic performance increase thanks to a morphing A320 wing with high-lift flap by means of CFD Hi-Fi approaches," *American Institute of Aeronautics and Astronautics*. https://doi.org/10.2514/6.2019-2912

[24] Marouf, A., Simiriotis, N., Tô, J. B., Bmegaptche, Y., Hoarau, Y., and Braza, M. 2019. DDES and OES Simulations of a Morphing Airbus A320 Wing and Flap in Different Scales at High Reynolds. Springer International Publishing, pp. 249–258. URL https://doi.org/10.1007/978-3-030-27607-2_20

.